Probing matter with electromagnetic waves / Sonder la matière par les ondes électromagnétiques

# A new technique to characterize foliage attenuation using passive radar in the L-band

## Nouvelle technique pour la caractérisation de l'atténuation par les forêts au moyen d'un radar passif en bande L

Marc Lesturgie [a,b,*], Laetitia Thirion-Lefèvre [b], Stéphane Saillant [a], Philippe Dorey [a]

[a] *ONERA–DEMR, Chemin de la Hunière, BP 80100, 91123 Palaiseau cedex, France*
[b] *CentraleSupélec, SONDRA, Plateau de Moulon, 3, rue Joliot-Curie, 91192 Gif-sur-Yvette cedex, France*

## A R T I C L E   I N F O

## A B S T R A C T

The goal of the experiment proposed in this paper is to give rapidly and with a limited equipment the attenuation level in the L-band for various elevation angles, between 20 and 70 degrees. The original principle is to use the L-band signal transmitted from an airport radar. The signal backscattered by a plane flying over the forest next to the airport is received on many antennas: some are over the canopy; others are on the ground under the foliage. The direct path signal transmitted by the airport radar is received by the antennas located above the forest. This signal is used to synchronize the temporal signals by detecting the waveform of the transmitting pulses. The signal backscattered by the plane is received by two H and V polar antennas located over the forest and by two other antennas placed under the foliage. The signals received by these antennas are digitized and processed to extract the plots of the opportunistic targets that approach the airport. The magnitudes of each plane echo are measured on each channel, and a comparison of the level of signal is made between the antenna above and under the forest. The ratio of magnitude between the two measurements on each polarization component gives the absorption factor of the foliage at the place of experiment. The position of the plane is given by an ADS-B receiver. For each elevation position of the antennas, the pattern of the chosen target will describe all the angles of arrival. This experiment has been deployed on two forested sites near an airport in South-East Asia.

## R É S U M É

L'expérimentation proposée dans cet article a pour but d'évaluer rapidement et avec un équipement limité le niveau d'atténuation dans la bande L pour différents angles d'élévation, entre 20 et 70 degrés. Nous avons utilisé pour cela le signal en bande L transmis par le radar d'un aéroport à proximité du site de mesure. Ce signal est ensuite

* Corresponding author at: ONERA–DEMR, Chemin de la Hunière, BP 80100, 91123 Palaiseau cedex, France.
*E-mail addresses:* marc.lesturgie@onera.fr (M. Lesturgie), laetitia.thirion@centralesupelec.fr (L. Thirion-Lefèvre), stephane.saillant@onera.fr (S. Saillant), philippe.dorey@onera.fr (P. Dorey).

diffusé par un avion survolant la forêt et est reçu sur plusieurs antennes : deux d'entre elles sont positionnées au-dessus de la canopée, tandis que deux autres sont posées au sol sous le feuillage. Le signal direct émis par le radar de l'aéroport est reçu par les antennes situées au-dessus de la forêt. Il est utilisé pour synchroniser les signaux temporels en détectant la forme d'onde des impulsions d'émission. Le signal diffusé par la carlingue de l'avion est receptionné par deux antennes de polarisation H et V situées sur la forêt et par deux autres antennes placées sous le feuillage. Les signaux reçus par ces antennes sont ensuite numérisés et traités pour en extraire les points de mesure correspondant aux cibles d'opportunité aux abords de l'aéroport. Les amplitudes des échos de chaque avion sont ainsi mesurées sur chaque canal de polarisation, et une comparaison du niveau du signal est effectuée entre l'antenne au-dessus et dans la forêt. Le rapport entre ces deux mesures pour chaque polarisation donne le facteur d'absorption du feuillage. La position de l'avion est donnée par un récepteur ADS-B. Pour chaque position d'élévation de l'antenne, le trajet de la cible choisie décrit tous les angles d'arrivée. Cette expérience a été déployée sur deux sites forestiers près d'un aéroport en Asie du Sud-Est.

## 1. Introduction

The purpose of this article is to investigate an outdoor measurement technique for a fast forest attenuation characterization with an easy set-up. The attenuation of a forest has a strong impact on the radar capabilities, whatever the application. Low-frequency radar systems are favored when penetration is required. As underlined in [1], HV data collected at P-band for instance have been demonstrated to be sensitive to above ground biomass variations, and the vertical structure of the forest can be investigated with Pol-InSAR data. For military application, in the frame of Foliage Penetration (FoPen) application, the attenuation of the crown is dramatically lowered when using frequencies typically ranging from 30 MHz to 1.2 GHz (VHF to L-band), which is expected to improve target detection. However, a trade-off between radar resolution and penetration has to be reached to enable detection and identification of targets concealed within forests. Solutions have been proposed to overcome this difficulty, either by increasing radar frequency as experimented by Nashashibi and collaborators [2] who used a 35 GHz radar or by specifically processing Synthetic Aperture Radar (SAR) signals to detect the target and extract its signature (for an example, see [3]). Several systems have been proposed to measure the attenuation of forests. We can quote for instance the ground-based measurements presented by Ulaby, Whitt and Dobson [4] or the system elaborated by Nashashibi and collaborators [2]. Either the one-way or the two-way attenuation is measured. In the first case, a transmitting antenna is deployed above the canopy, and a receiver is located below. In the second case, we are in monostatic configuration with a transmitter/receiver above the canopy and a calibrated target (active or passive) within the canopy. The antennas located above the crown can be mounted on a truck or on a crane for instance. Because of the spatial inhomogeneity of the forests, a variation of the attenuation throughout the canopy is expected. This variability can be partly measured as in [4] or [2] either by rotating the antenna—keeping the incidence angle constant but with a varying azimuthal angle—or by moving the receiver–target couple to characterize different locations. The level of the calibrated target can be measured by placing the corner reflector—for instance—outside the forest. Regarding the attenuation measurements with airborne radar, it is difficult to characterize the variability of the forests as only some corner reflectors can be deployed within and outside the forests. In this last case, neither the space- nor the time-variabilities are generally taken into account. However, these variabilities are typical of natural environments, and for that reason, we will not look for a single attenuation coefficient, but rather for a statistical distribution. Therefore, this characterization requires a large number of radar data and the purpose of this paper is to present an experiment adapted to these requirements and easy to set up.

The second section of this paper states the principle of our experimental set-up, then we present the configuration of the data collected near an international airport, in South-East Asia. Section 3 is dedicated to the processing, and some of our assumptions are further investigated. Finally, the measurements are analyzed and compared with simulated data.

## 2. Principle

We present in this paper a novel approach that uses a passive radar technique, fully mastered by ONERA—the French Aerospace—and usually operated for target detection. The objective here is not to detect and locate targets, as we perfectly know them: they are civil aircrafts localized by means of ATM (Air Traffic Management) calendar. We use this knowledge to evaluate the properties of the propagation channel. As we would do in the frame of FoPen application—foliage penetration mode suitable to low-frequency airborne radars for ground monitoring—we deploy a system with two receiving systems located at different heights. The upper system, above the canopy, collects reference signals. We assume that these signals are free of any attenuation or scattering effect due to foliage). The lower system, below the canopy, collects the attenuated signals (see Fig. 1).
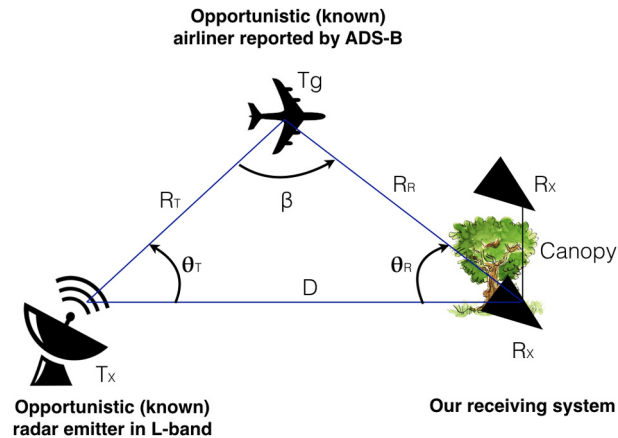
**Fig. 1.** The radar airport illuminates the planes, which in turn act as secondary sources. The signal coming from the plane is of unknown elliptic polarization. This signal is then collected by two receiving systems, but with the same receiving angle, because of the far-field condition: the first one, above the canopy, is the reference signal; the second one, below the canopy, is the signal attenuated by the forest.



**Fig. 2.** Typical type of vegetation in the first test site.

Actually, each receiving system is composed of two antennas: one vertically polarized, the other horizontally polarized. The broadcasted signal is provided by any neighbor transmitter in the band of interest, for instance a radar airport. Actually, next to an airport, the aircrafts traffic is dense and the planes can be used as secondary radar sources of arbitrary polarization. They fly over the forest in a bistatic configuration and allow one, by reflection, to collect two time series of echoes: one above the canopy, the other one below. The receiving angles are expected to be the same for both antennas as we assume that we are in a far-field configuration. In addition, as the aircraft moves toward (or backward) the airport, the receiving angle varies. This time variation is interesting as we can study the variation of attenuation depending on the angle of incidence. When the configuration is well chosen, thousands of data can be collected, allowing statistical analysis. Furthermore, as we operate differential measurements between the antennas below and above the canopy, we can neglect the scattering pattern of the planes in a first approximation.

## 3. Measurements

### 3.1. Test sites

Two sites have been selected near the international airport with two types of vegetation:

- the first site is just at the south-east from the airport where the planes are taking off or landing on the main track. At this place, trees are around 20 m high and vegetation is not quite dense. The forest is constituted of pine trees and broad-leaved trees, as shown in Fig. 2. A boom crane has been used to place the antennas above the canopy, as shown in Fig. 3;

**Fig. 3.** First test site at the south-east of the airport. The above-crown receiving antennas have been placed on the boom crane.



**Fig. 4.** Typical type of vegetation in the second test site.
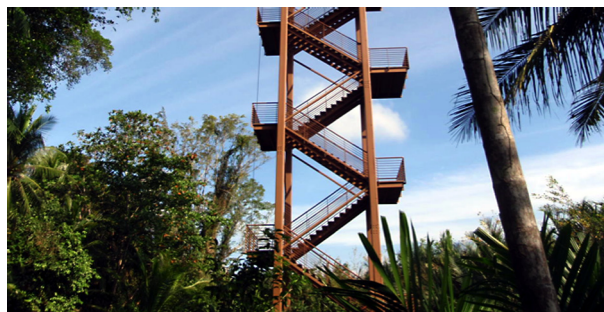


**Fig. 5.** Scenic viewing tower in the second test site.

- the other site is facing the airport radar used as an opportunistic transmitter. Fig. 5 shows a 21-m-high scenic viewing tower that was used to place the antennas above the trees. The vegetation is rather dense, with different heights of trees as a function of the direction (Fig. 4). In the north and east directions, it is a mangrove type of trees, with a maximum height around 10 m. Heights are higher in the south and west directions, with trees that can be 20 m high.

The distances from the airport transmitter and the receiving antennas are respectively 8.3 km for the first test site and 2.3 km for the second one.

**Table 1**
Specifications of the airport radar.

| | |
|---|---|
| Radar type | TRAC 2400 |
| Antenna gain | 36 dB |
| Antenna rotation rate | 6 rpm |
| Frequencies | 1265, 1270, 1315, 1320 MHz |
| PRF 1 | 267 Hz |
| PRF 2 | 309 Hz |
| PRF 3 | 257 Hz |
| PRF 4 | 300 Hz |
| Short pulse width | 1 μs |
| Long pulse width | 100 μs |
| Peak power | 36 kW |

**Table 2**
Characteristics of the log-periodic antennas.

| | |
|---|---|
| Frequency band | [1.2, 3] GHz |
| Polarization | linear |
| Impedance | 50 Ω |
| VSWR | < 2 |
| Gain | > 7.5 dBi |
| Beamwidth in H-plane | > 90° |
| Beamwidth in E-plane | > 48° |

### 3.2. Airport radar specifications

This radar operates in the L-band and transmits 4 frequencies:

- 1265 MHz, with long pulses,
- 1270 MHz, short pulses,
- 1315 MHz, long pulses,
- 1320 MHz, short pulses.

It uses four Pulse Repetition Frequencies (PRF) successively transmitted in series of 8 or 10 pulses for each radar frequency. All the specifications of the radar are given in Table 1.

### 3.3. Receiving antenna specifications

Four identical Log-periodic antennas are used to receive the signal on each channel: two for horizontal polarization and two for vertical polarization. Each pair of (H, V) antennas is located above and below the canopy. The characteristics of these antennas are given in Table 2.

The radiation pattern of the antennas has been measured for H- and E-planes and are given in Fig. 6.

### 3.4. ADS-B receiver

As the planes around the airport are used as targets, we had to know their exact patterns to extract their echoes in the receiving signal. This could be a complicated task because of multipath propagation. However, we had at our disposal the ADS-B (Automatic Dependent Surveillance-Broadcast) information. It allows us to select a single plane, to follow its trajectory on the map provided by ADS-B and to calculate its delay (see Fig. 7). In this way, we can assess which peak is associated with the plane of interest. This has been done with an ADS-B receiver, which allows us to have the air situation in real time and to record the positions of all the planes around.

In order to get targets that describe all the elevation angles, an ADS-B receiver has been used to select the azimuth directions to which the antennas have to be pointed in order to keep the planes in the main lobe as long as possible.

After a survey period of the air traffic at the beginning of the experiment campaign and in order to cover all the elevation coverage, we chose to work mainly with planes flying at high altitudes, whose pattern passes just above the receiving place.

### 3.5. Configuration

The direct path transmitted by the airport radar is received on the antennas positioned above the canopy (see Fig. 1). The signal of the radar airport is then diffracted by the aircraft and is finally received by two antenna pairs in H and V polarization (see Fig. 8). These antennas are positioned below and within the canopy. We assume that the distance between the airport radar and all the receiving antennas is the same and is equal to *D*. We need to estimate the distance

**H**

LOG-1.2-3GHZ.N4W Azimuth Total Field
Frequency = 1300.000 MHz
Antenna in Free Space
Z1 = 80.11 + j8.62 (1.63)
Zenith Angle = 0 deg.
Max = 7.85 dBi
F/B = 24.26 dB

0 dB = 7.85 dBi
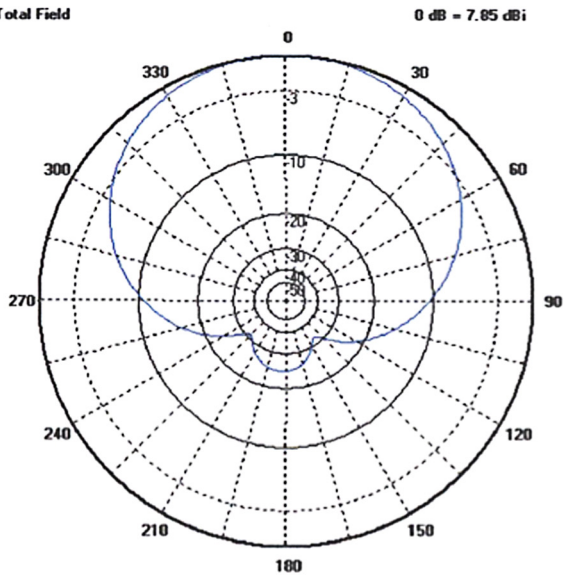
**E**

LOG-1.2-3GHZ.N4W Zenith Total Field
Frequency = 1300.000 MHz
Antenna in Free Space
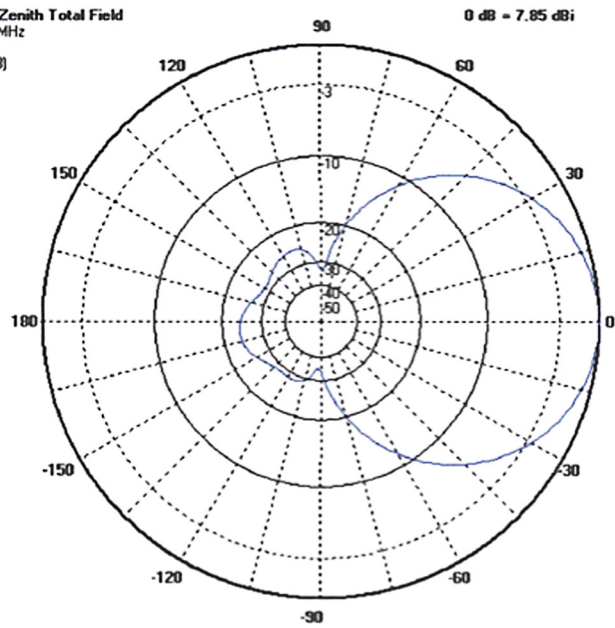Z1 = 80.11 + j8.62 (1.63)
Max = 7.85 dBi

0 dB = 7.85 dBi

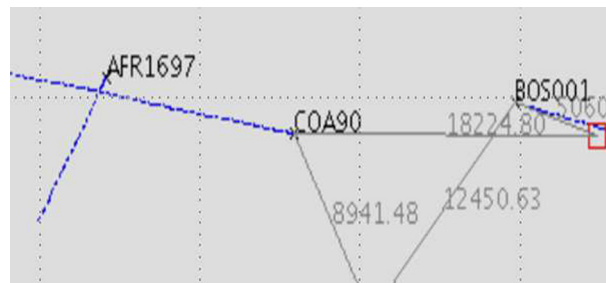**Fig. 6.** Antenna pattern in H-plane (top) and in E-plane (bottom).

**Fig. 7.** Typical information generated by the ADS-B receptor, which allows us to identify the plane.

**Fig. 8.** Each receiving system—above and below the canopy—is comprised of two antennas: one vertically polarized, the other one horizontally polarized. The signal coming from the plane if of unknown polarization. When it is collected by the receiving systems, the antennas act like filters, so that one can determine the attenuation for the two copolarizations.
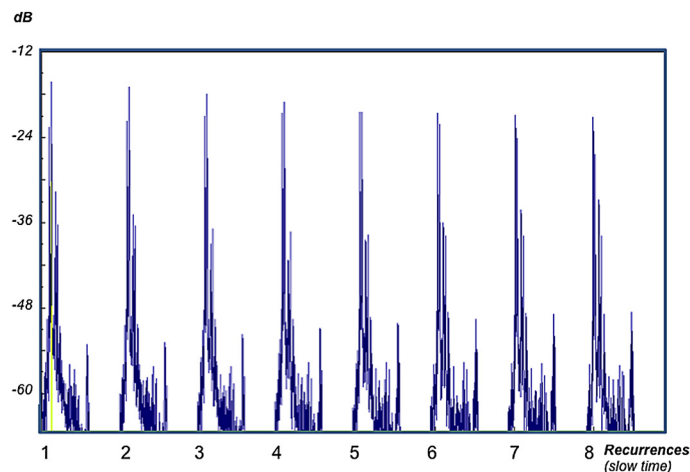


**Fig. 9.** Time signal emitted by the radar airport.

and to measure the angle of arrival of the target echoes. Bistatic distance is given by the measurement of the propagation time from transmitter to target to receiver. This time measurement is converted to a distance ($R_T + R_R$), where $R_T$ is the transmitter-to-target distance and $R_R$ is the target-to-receiver distance. For distance measurement, it is needed to synchronize the signals. As the TRAC 2400 radar of the airport uses a rotating aerial, it is necessary to provide synchronization between transmitting and receiving with respect to the direct path azimuth.

During all trials, the air traffic was recorded with an ADS-B receiver. A real-time research of the best planes for a maximum scan of elevation angles was done to optimize the focalization of the antennas. The antennas were oriented in the direction for which the selected target would remain as long as possible in the main lobe, with an evolution along a maximum of angle of arrival.

### 3.6. Processing

The processing and acquisition system includes four completely independent channels that record all signals over a very long time.

#### 3.6.1. First step: synchronization and radar code recovering

The digitized signal received on each channel contains the direct path and the closed ground echoes, as illustrated in Fig. 9. The PRF of the radar can be measured and the time between each peak is 3.33 ms, leading to 300 MHz (PRF 4). The direct path is then extracted (see Fig. 10) and can be used to synchronize the receiving radar signals.
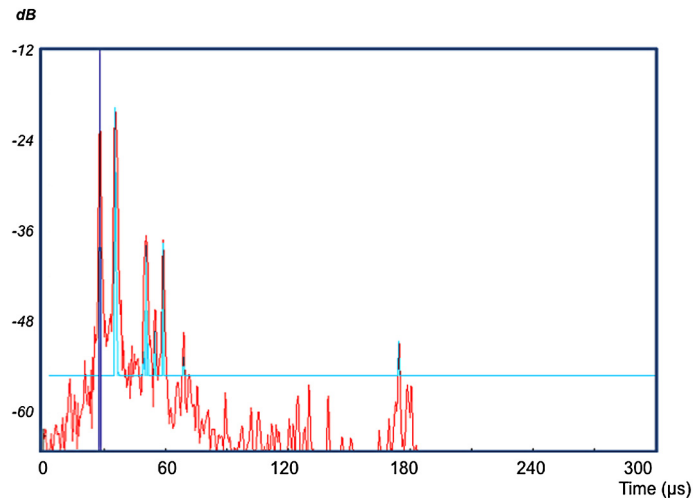
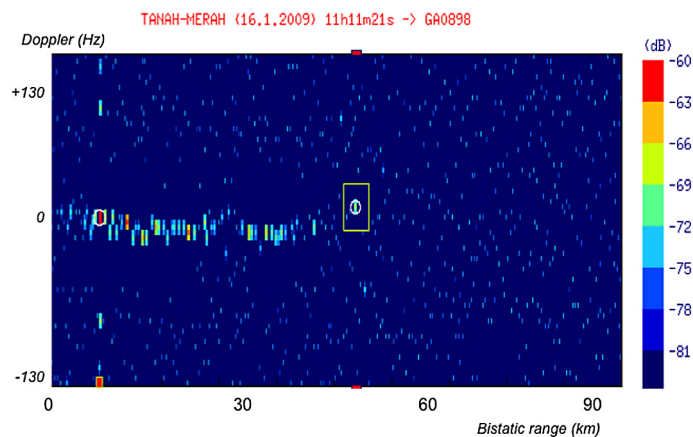**Fig. 10.** Direct path received by the above antenna in the time-domain.



**Fig. 11.** Example of a range-Doppler image of the collected echoes after synchronization. The signature of the aircraft is indicated by the yellow rectangle.

### 3.6.2. Second step: long-time data collection

As mentioned before, two antenna pairs (H and V polarization) are positioned below and above the canopy. As a result, the signals are recorded on four completely independent channels. A long time record is achieved in order to collect data with varying positions of the aircrafts. Consequently, we can collect numerous values of attenuation at H and V polarizations for various elevation angles typically ranging from 20 to 70 degrees.

### 3.6.3. Third step: range processing

Because of the bistatic configuration, the direct path has to be detected and in particular its time of arrival.

The first signal is of high amplitude as it is the direct path (see Fig. 10). It may be followed by strong signals especially when the primary radar beam is not oriented in the direction of the measuring system. In this case, multipath radars can lead to strong returns that can be at about the same level as the direct path.

Once the direct path detected and its peak well positioned in the time series, we need to identify the echoes of the planes.

### 3.6.4. Fourth step: Doppler processing

The target of interest chosen from the ADS-B pattern is identified and its position is refined in range. An example is given in Fig. 11, representing a range-Doppler image after synchronization with the direct path. The target is within the yellow rectangle. Doppler processing is a coherent step that requires to process the phase of each received pulse. As the primary radar has no physical link with the receiving station, we have to retrieve the phase of each transmitted pulse. This is done from the direct path signal, which is not affected by the Doppler effect. The phase measured from the direct path signal is then subtracted from the phase of the target echo. Once the compensation is performed, the residual phase is only due to the motion of the target.
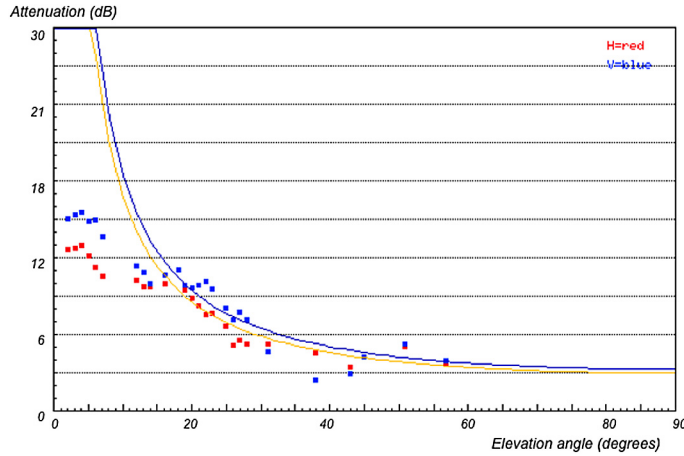
**Fig. 12.** Variation of foliage attenuation with the elevation angle for the first test site. Red color codes indicate H polarization and blue color ones V polarization.

Due to the bistatic geometry, the bistatic Doppler shift is not simply related to the radial velocity of the target M, as in the conventional monostatic radar. Here, the Doppler shift is equal to:

$$F_{\text{dop bistatic}}(M) = \frac{1}{\lambda} \vec{V}_M \cdot \vec{U}_{\text{EM}} + \frac{1}{\lambda} \vec{V}_M \cdot \vec{U}_{\text{RM}} \tag{1}$$

where $\vec{V}_M$ is the target velocity vector, $\vec{U}_{\text{EM}}$ and $\vec{U}_{\text{RM}}$ are the unit vectors in the directions of the emitter (radar) and of the receiver. The ADS-B information is used to calculate the expected Doppler shift. The Doppler processing is performed using a Fast Fourier transform. Both expected and extracted (measured) Doppler values are jointly used to confirm and localize the echo of interest in the range-Doppler map. We see also in Fig. 11 the distribution of the multipath echoes (the clutter) around a zero-Doppler axis.

## 4. Data analysis

### 4.1. Variation of the attenuation over the depression angle

The number of collected data is huge (typically proportional to the number of flying aircraft around or over the area) which is interesting to get different incidence angles and perform statistical analysis. In a first approach, data collected within each sector of incidence (typically a few degrees) can be averaged to get a confident value. Further analysis of the data might also include the derivation of the statistics. This is not described in this paper. Thanks to the proposed method, the angle diversity is important: from 3° to 70° of depression angle associated with an airliner route of several tens of kilometers. Two sites have been considered. The first site is a mangrove forest. The second one is a forest of mixed pines trees. All the data from all the files have been concatenated to present a global view of the measurements of attenuation through the foliage for each site of experiment. Raw data have been collected on the two sites after a processing of filtering by using only the data with a signal-to-noise ratio (SNR) over 6 dB. Then, we have selected the measurements obtained simultaneously n H and V polarization, and finally we have applied a weighting window over 10-degree elevation. The final results are presented in Fig. 12 for the first test site and 13 for the second one.

While the loss increases as the depression angle decreases (at grazing), the use of horizontal polarization is always more favorable. We also notice more prominent loss for the mangrove-kind forest (second site).

### 4.2. Interpolation and filtering of the data

The Figs. 12 and 13 also display a set of curves that result from interpolating the data. An interpolation is proposed, based on a simple approach. Assuming that the forest is defined by its height $h$, the travel distance of the wave through the forest is function of the angle of arrival and is given by:

$$D_i = \frac{h}{\sin \phi_i} \tag{2}$$

where $\phi_i$ is the depression angle (and $\phi_i \ll 1$ at grazing). Assuming a model of transmission line with an attenuation $L_{\text{lin}}$ (in dB per meter), we obtain the total attenuation:

$$L_{\text{Fop}}(\phi_i) = L_{\text{lin}} D_i = L_{\text{lin}} \frac{h}{\sin \phi_i} \tag{3}$$
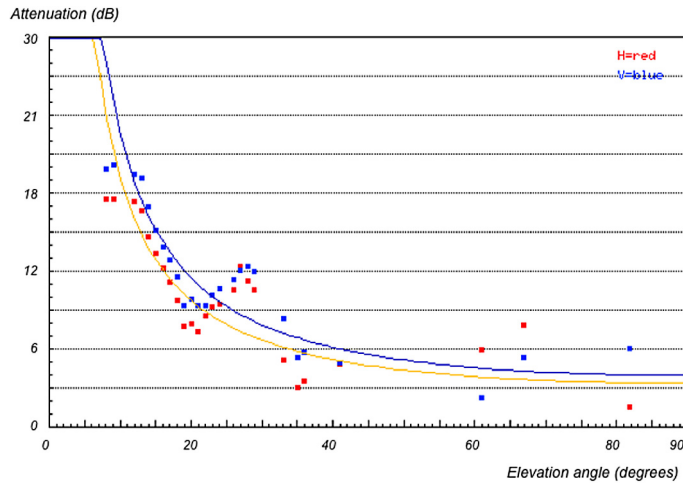
**Fig. 13.** Variation of foliage attenuation with the elevation angle for the second test site. Red color codes indicate H polarization and blue color codes V polarization.
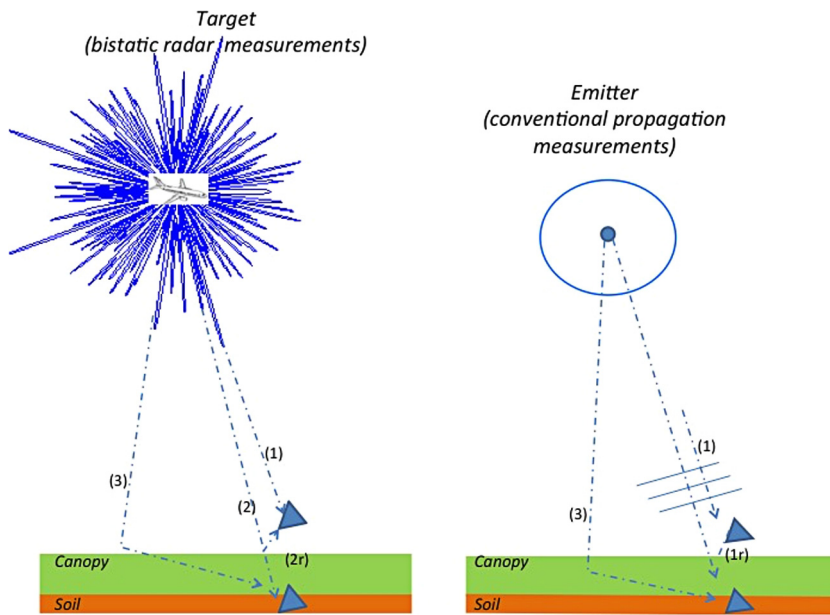


**Fig. 14.** Comparison of the two configurations: (right) conventional case where the emitter is a radar antenna located in the far field of the target; (left) bistatic and passive case where the plane body is used as a secondary emitter.

or

$$L_{\text{Fop}}(\phi_i)\sin\phi_i = L_{\text{lin}}h \tag{4}$$

Thanks to the ADS-B information, all the ground truth parameters are retrieved, including the depression angle $\phi_i$. Then we can average the first part of the last equation for all the data corresponding to the elevation $\phi_i$ and finally compute the fitting filtered curves (solid lines) based on real data.

### 4.3. Effect of the target diffraction and limitation

Opportunistic airliners are used as secondary emitters. The diffraction pattern of the airliners is unknown; however, the radar signature received is assumed to be the same on the two antennas. Any difference in target signature may affect the estimation of the propagation loss.

Fig. 14 summarizes the different mechanisms and also illustrates the main difference between the proposed method and the conventional use of a almost-isotropic transmitting antenna for the characterization of the FoPen attenuation. In this figure:
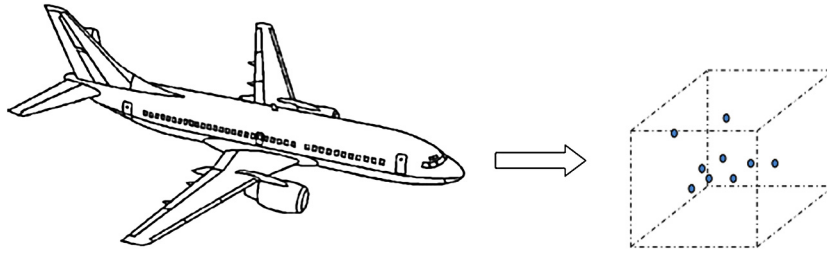
**Fig. 15.** A simple model to represent the scattering by a non-punctual target.

- path (1) and path (2) carry the signals of interest with eventually two different target signatures, due to the near-field effect,
- path (3) penetrates the canopy under an unexpected direction, benefiting from a high-level diffraction lobe (this path may not exist in conventional scenario, or may exist with a much weaker level),
- path (2r) is a reflection in the vicinity of the upper antenna.

This target diffraction effect can be seen as a near-field effect in relation with the size of the target and the wavelength. A complete analysis of this effect would require a coherent modeling of the bistatic diffracted field. A simple analysis is proposed hereafter. To appreciate this impact of the target diffraction on the measurement of interest (foliage attenuation), we consider a simple target model based on a finite number of scattering centres spread in a cube having the size of the overall dimension of the aircraft (Fig. 15). We do not consider the vegetation layer here, to precisely assess the impact of target diffraction aspects alone. Therefore, each scatterer is considered as a secondary emitter which contributes to the following received signals:

$$S_p = \alpha \sum_i a_i \exp\left(jM_i R_p\right) \tag{5}$$

with $p = 1$ for the upper antenna, $p = 2$ for the lower antenna and:

- $S_p$ is the complex signal received on each channel ($p = 1, 2$),
- $\alpha$ is a constant; antenna pattern and gain are assumed to be identical on each channel ($p = 1, 2$),
- $a_i$ and $M_i$ are the amplitude and position of the scattering centres,
- $R_p$ is the position of the receiving point.

In the absence of vegetation, the power difference between the two antennas is simply equal to:

$$\beta_{\mathrm{dB}} = 20 \log_{10} \left| \frac{S_2}{S_1} \right| \tag{6}$$

A statistical simulation has been performed, based on different sets of position and amplitude of the scattering centres within a volume area which corresponds to the overall size of an airliner. This approach is more statistical than physical: the position of the scattering centres is randomly chosen within the cube (Fig. 15). Then we evaluate the statistics of the error and compute the cumulative distribution function of $\beta_{\mathrm{dB}}$ from a Monte Carlo simulation based on several tens of thousand of runs. Fig. 16 shows cumulative distribution function for two incidence angles (9° and 69°). For high incidence (low depression/grazing angle) the error on the attenuation in 80% of the cases can raise 5 dB for a short range of 5 km. Longer the range, lower the error, which finally becomes negligible in far-field conditions.

We can now pay more attention to grazing angles and to the geometry of the airliner routes used for the derivation of the attenuation. The top of Fig. 17 displays the measured attenuation, the airliner route and the distribution of the error, according to the previous statistical modeling. In this example, the aircraft is an Airbus A330 (large size, for which we consider a cluster of scattering centres within a 40-m-edge cube). The difference of height between the lower and upper antennas is 20 m. At 43 km and a grazing angle, the error should be less than 2 dB (at 90%). At 4° grazing angle, due to the shorter distance (19 km), the error is statistically twice, around 4 dB. The bottom of Fig. 17 shows similar results for a smaller aircraft (A320, represented by a 30-m-edge cube) at a shorter distance. At 23 km and grazing angle, the error should be less than 2.5 dB (at 90%) At shorter distance (13 km), the error raises to 3 dB.

## 5. Modeling

In order to further assess the relevancy of the measurements, some simulations have been performed using COSMO [5]. This code has been developed in order to study and analyze the backscattering by forested areas for FoPen applications.
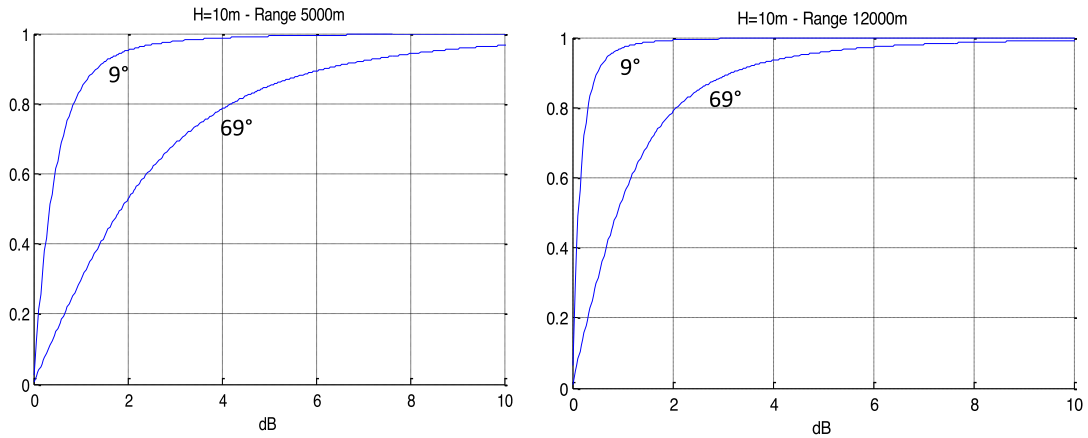
**Fig. 16.** The cumulative distribution function of the error $\beta_{dB}$ for two different ranges and two different depression angles: 9° (left) and 69° (right).
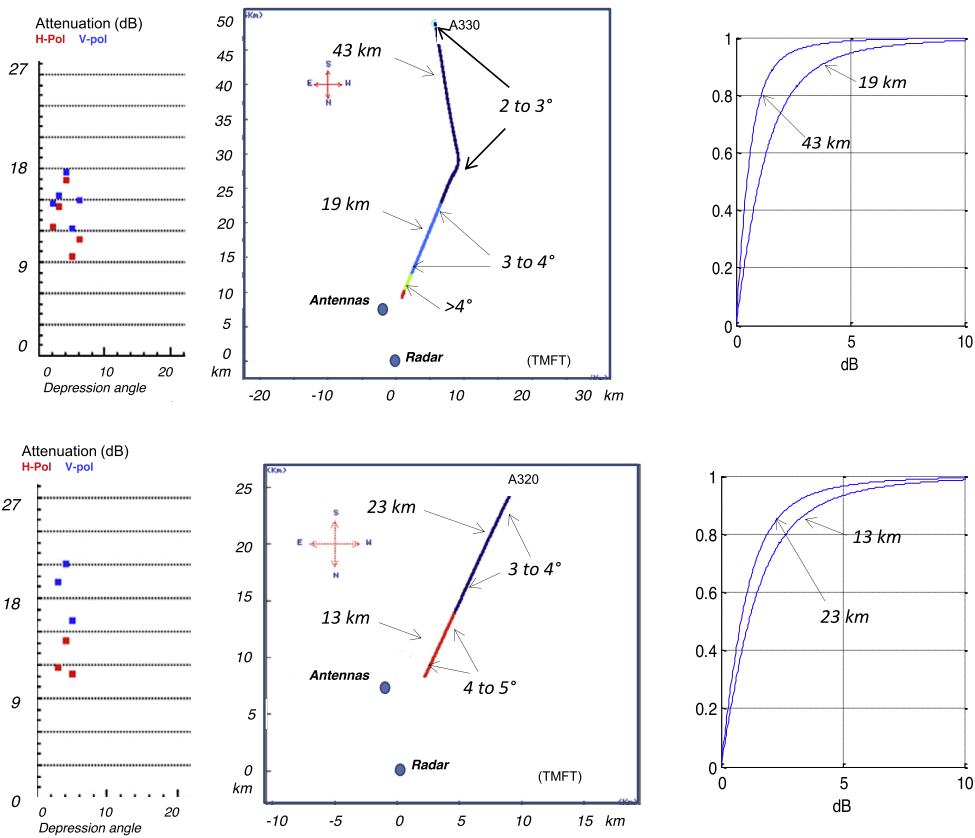


**Fig. 17.** Analysis of the attenuation error due to diffraction effects for two examples at grazing angles: A330 (top), A320 (bottom). For each example, the measured attenuation (left), the airliner route (middle) and the distribution of the error (right) are given.

## 5.1. Short description of COSMO

This asymptotic tool has been validated for various configurations (radiometry, polarimetry, interferometry; at P- and L-bands; for different incidence angles and for different kinds of forests; see [5] for a detailed description). For that reason, it is a good candidate to test the relevancy of the measured attenuation. Previous works have been dedicated to the validity of the attenuation simulated by COSMO [5], as well as its spatial distribution and its variation with frequency and incidence angle [6,7]. COSMO creates first a forested scene where trees are roughly described using dielectric cylinders and ellipsoids. The density of these scatterers is provided for each layer and each group of tree elements (naked trunks, primary branches, secondary branches, twigs and leaves or needles). The moisture content is required for the vegetation and the ground, so
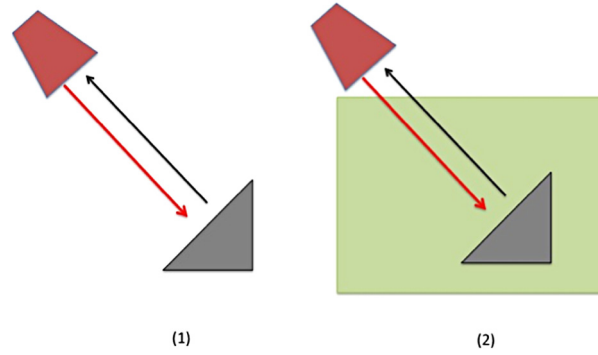
**Fig. 18.** Illustration of the simulation of the attenuation. A measurement of the received field is performed without (1) and with (2) vegetation.

that the permittivities can be calculated for each frequency and ambient temperature. Finally, the electrical field is simulated for the whole scene for all linear polarizations, given the radar frequency and the incidence angle.

### 5.2. Principle of the simulation

The total attenuation is simulated as follows: the free-space response of a corner reflector (1) is compared to the response of the same corner reflector, when located inside the forest (2), as represented in Fig. 18. There are as many reflectors as trees and the backscattered field of each of them is simulated inside COSMO by implementing the literal expression of their highest contribution [8]. Thus, the total attenuation $A_{\mathrm{Np}}$ in linear scale is defined as:

$$A_{\mathrm{Np}} = 2\alpha d = -\ln\left(\frac{|E_{qp}^{\mathrm{s,att}}|^2}{|E_{qp}^{\mathrm{s,non\ att}}|^2}\right) \tag{7}$$

$d$ is the one-way through the forest, so $2d$ is the two-way through the forest, $\alpha$ is the line attenuation (Np/m), $|E_{qp}^{\mathrm{s,att}}|^2$ is the intensity that we measure within the forest and $|E_{qp}^{\mathrm{s,non\ att}}|^2$ is the intensity that we measure outside the forest. In these expressions, $E$ is the electrical field and $q = v, h$ and $p = v, h$ are the incident and backscattered polarizations.

The total attenuation $A_{\mathrm{dB}}$ is defined as (dB):

$$A_{\mathrm{dB}} = \frac{10}{\ln 10} A_{\mathrm{Np}} \tag{8}$$

The line attenuation is derived therefore from $A_{\mathrm{Np}}$:

$$\alpha = -\frac{1}{2d}\ln\left(\frac{|E_{qp}^{\mathrm{s,att}}|^2}{|E_{qp}^{\mathrm{s,non\ att}}|^2}\right) \tag{9}$$

The way the attenuation is simulation with COSMO gives actually the two-way attenuation. In the experiment, the one-way attenuation has been measured. For that reason, we have to consider $A_{\mathrm{Np}}/2$ instead of $A_{\mathrm{Np}}$.

### 5.3. Description of the two test sites

The difficulty is that no ground truth data collection has been performed on the two test sites during the radar data collection, except for the mean height of the trees. As we need a detailed description to run COSMO, we have considered two types of forest, which seem to be closed to those observed during the ONERA campaign:

- the first test site is similar to a pine-tree forest with sandy ground and is 18 m high;
- the second test site is similar to a Mangrove and is 18.5 m high.

These two types of forests have been already studied in previous projects (see [5]), so that we can provide some typical characteristics to describe these two sites as a first approximation to evaluate the attenuation. Some modifications have been applied to take into account the temperature and the moisture of the scene, which can be estimated as the weather is relatively constant in this location. For both stands, the moisture has been set to 70% and the temperature to 30°. The resulting dielectric permittivities at 1.2 GHz are given in Table 4. These stands and their ground are respectively described in Tables 3 and 5. As explained above, the calculation of the attenuation has been simulated using ideal corner reflectors spread in the stands. We have computed their response within and outside the forest and therefore we have deduced the attenuation. Border effect have been suppressed. In addition, we do not have considered the effect of the needles or leaves, as previous studies have shown that this would lead to an important overestimation of the attenuation, whereas without them, we had a slight underestimation of the attenuation [5].
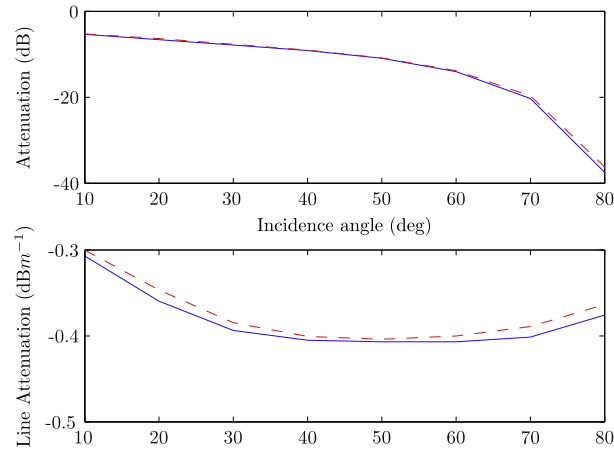
**Fig. 19.** Variation with the incidence angle of the total (top) and line (bottom) attenuation simulated over a pine-tree forest in VV polarization (solid blue line) and in HH-polarization (dashed red line).
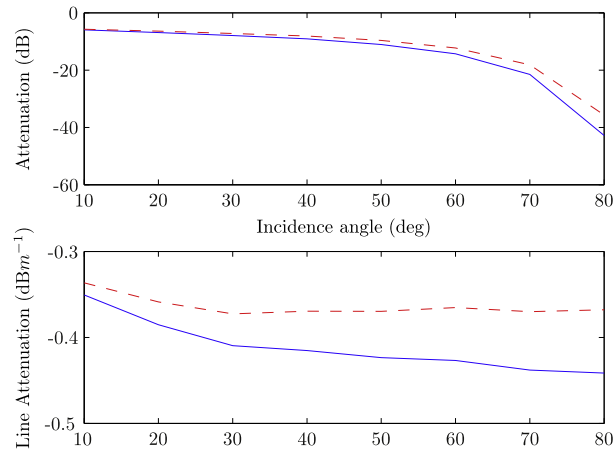


**Fig. 20.** Variation with the incidence angle of the total (top) and line (bottom) attenuation simulated over a mangroves-type forest in VV polarization (solid blue line) and in VH-polarization (dashed red line).

**Table 3**
Description of mangrove-type and pine-tree forest stands: $H$ is the height of the layer (meter), $h$ and $r$ are the height and the radius of the branches and of the trunks (respectively in meters and centimeters), whereas $\mathcal{D}$ is the volume density of each type of scatterer (number of elements per meter). The Eulerian angles are defined as follows: $\alpha \in [0°, 360°[$ for all scatterers; $\beta$ is specified for each case.

| Type | Mangroves | Pine trees |
|---|---|---|
| Layer 1 | $H = 8$ | $H = 11$ |
| trunks | $h = 8; r = 23.4$<br>$\mathcal{D} = 0.00089$<br>$\beta_{min} = 0°$, $\beta_{max} = 10°$ | $h = 11; r = 14.5$<br>Spacing = 4.4<br>$\beta_{min} = 0°$, $\beta_{max} = 10°$ |
| Layer 2 | $H = 6$ | $H = 7.5$ |
| trunks | $h = 6; r = 13.5$<br>$\mathcal{D} = 0.00089$<br>$\beta_{min} = 0°$, $\beta_{max} = 10°$ | $h = 7.5; r = 4.6$<br>Spacing = 4.4<br>$\beta_{min} = 0°$, $\beta_{max} = 10°$ |
| branches | $h = 2.5; r = 1.5$<br>$\mathcal{D} = 0.208$<br>$\beta_{min} = 0°$, $\beta_{max} = 90°$<br>$h = 1.5; r = 0.4$<br>$\mathcal{D} = 2.06$ | $h = 2.2; r = 1.2$<br>$\mathcal{D} = 0.38$<br>$\beta_{min} = 40°$, $\beta_{max} = 80°$<br>$h = 0.22; r = 0.32$<br>$\mathcal{D} = 5.60$ |
| Layer 3 | $H = 4$ | |
| branches | $h = 1; r = 1.1$<br>$\mathcal{D} = 0.094$ | |

**Table 4**

Relative complex permittivities for mangrove and pine-tree forest stands in the L-band.

|  | Mangrove stands | | Pine-tree stands | |
|---|---|---|---|---|
|  | Ground | Vegetation | Ground | Vegetation |
| L-band | 54–j 5.2 | 28.8–j 9.2 | 37.32–j 2.26 | 19.87–j 6.73 |

**Table 5**

Roughness parameters for mangrove and pine-tree forest stands. The root mean square height ($h_{\mathrm{rms}}$) and the correlation length ($l_{\mathrm{c}}$) are given in centimeters.

|  | Mangrove stands | Pine-tree stands |
|---|---|---|
| $h_{\mathrm{rms}}$ (cm) | 1.7 | 10 |
| $l_{\mathrm{c}}$ (cm) | 10 | 100 |

### 5.4. Summary of the results

The total attenuation (as shown on Fig. 19 and Fig. 20) for the pine-tree forest and the mangrove-type forest varies between −6 dB and −20 dB for elevation angles in $[10, 70]°$. For the line attenuation, we have to consider separately the pine-tree forest (test site 1) and the mangrove-type forests (test site 2). For the first test site, it evolves from $-0.3$ dB m$^{-1}$ to $-0.4$ dB m$^{-1}$ from 10° to 30° and then stays constant until 70°. The co-polarizations behave similarly. For the second test site, the VV attenuation (evolving from 0.35 dB m$^{-1}$ to 0.45 dB m$^{-1}$) is more important than the HH attenuation (around 0.34 and 0.37 dB m$^{-1}$).

It can be noticed that the measurements are in agreement with the simulations. The horizontal attenuation is lower than the vertical one, the values are consistent, as well as their variation with the incidence angle (for reminding, the incidence angle is the complementary to the elevation angle).

### 6. Conclusion

We presented in this paper an original method for characterizing radio-wave attenuation using a passive system. This method has been tested and validated on a FoPen configuration and for two test sites. The configuration of the experiment has been presented in details and discussed as well. In addition, the measured values have been confronted to simulated attenuations, and it appeared that the values as well as the variation with the incidence angle and between polarizations were similar. This kind of experiment could be applied and extended to other applications where it is necessary to collect a large number of radar data using bistatic radar either in a passive configuration—if there is an existing transmitter—or an active configuration—by adding a cooperative transmitter.

### References

[1] F. Garestier, T. Le Toan, Estimation of the backscatter vertical profile of a pine forest using single baseline P-Band (Pol-)InSAR data, IEEE Trans. Geosci. Remote Sens. 48 (9) (2010) 3340–3348, http://dx.doi.org/10.1109/TGRS.2010.2046669.

[2] A. Nashashibi, K. Sarabandi, S. Oveisgharan, M. Dobson, W. Walker, E. Burke, Millimeter-wave measurements of foliage attenuation and ground reflectivity of tree stands at nadir incidence, IEEE Trans. Antennas Propag. 52 (5) (2004) 1211–1222, http://dx.doi.org/10.1109/TAP.2004.827250.

[3] F. Brigui, L. Thirion-Lefevre, G. Ginolhac, P. Forster, New SAR algorithm based on orthogonal projections for MMT detection and interference reduction, IEEE Trans. Geosci. Remote Sens. 52 (7) (2014) 3800–3811, http://dx.doi.org/10.1109/TGRS.2013.2276417.

[4] F. Ulaby, M. Whitt, M. Dobson, Measuring the propagation properties of a forest canopy using a polarimetric scatterometer, IEEE Trans. Antennas Propag. 38 (2) (1990) 251–258, http://dx.doi.org/10.1109/8.45128.

[5] L. Thirion, E. Colin, C. Dahon, Capabilities of a forest coherent scattering model applied to radiometry, interferometry, and polarimetry at *p*- and *l*-band, IEEE Trans. Geosci. Remote Sens. 44 (4) (2006) 849–862, http://dx.doi.org/10.1109/TGRS.2005.862523.

[6] L. Thirion-Lefevre, E. Colin-Koeniguer, Investigating attenuation, scattering phase center, and total height using simulated interferometric SAR images of forested areas, IEEE Trans. Geosci. Remote Sens. 45 (10) (2007) 3172–3179, http://dx.doi.org/10.1109/TGRS.2007.904921.

[7] A. Vasko, L. Thirion-Lefevre, S. Bilicz, I. Champion, M. Lambert, S. Gyimothy, Metamodel-based adaptive use of a coherent polarimetric backscattering simulator for the characterization of forested areas at low frequencies, in: PIERS Proceedings, Suzhou, China, 2011, pp. 818–822.

[8] F. Ulaby, C. Elachi, Radar Polarimetry for Geoscience Applications, Artech House, Norwood, 1990.